J. Fluid Mech. (1991), *vol.* 223, *pp.* 457–474
Printed in Great Britain

Time-periodic convection in porous media: the evolution of Hopf bifurcations with aspect ratio

By D. S. RILEY[1] AND K. H. WINTERS[2]

[1]School of Mathematics, University of Bristol, University Walk, Bristol BS8 1TW, UK
[2]Theoretical Studies Department, Harwell Laboratory, Didcot, Oxon OX11 0RA, UK

(Received 26 April 1990)

Techniques of bifurcation theory are used to study the porous-medium analogue of the classical Rayleigh–Bénard problem, Lapwood convection in a two-dimensional saturated porous cavity heated from below. The focus of the study concerns the destabilization, through symmetry-preserving Hopf bifurcations, of the various stable convective flow patterns that can form in a rectangular cavity. We show how the limits of stability of steady convection in a porous medium can be determined by bifurcation techniques that locate Hopf bifurcations, and we predict a surprisingly complex evolution of the Hopf bifurcation along the unicellular branch as the aspect ratio varies. The continuation methods that we adopt reveal interactions of Hopf bifurcations with limit points that signal complicated dynamical behaviour for certain container sizes. The study demonstrates the role of Hopf bifurcation in destabilizing completely the unicellular flow at aspect ratios greater than 2.691. A simple relationship between symmetry-preserving Hopf bifurcations from the alternative steady flows is also derived, and used to define upper limits on the stability of the alternative steady flows and the thresholds for oscillatory convection as a function of aspect ratio.

1. Introduction

There have been numerous studies over the years of natural convection inside a two-dimensional rectangular saturated porous cavity heated from below (see Bories 1985). The majority of past studies have concentrated on steady flows in cavities of varying aspect ratio and isothermality conditions. The problem of transition to, and evolution of, unsteady flow has, in comparison, received much less attention. Moreover, past studies of the transition problem (see Aidun & Steen 1987), have been adversely affected by inaccurate calculations and much uncertainty about the results. In the main, the causes have been two-fold: first the resolution of the finite-difference/element grids has been poor (owing, in part, to limitations on computing capacity). Secondly, most of the calculations have been based on time-dependent codes and so the transition point has been inferred from an observed change from damped-oscillatory to true-oscillatory behaviour as the Rayleigh number increases.

In recent times this particular porous-medium problem has become recognized as an important prototype for a class of (hydrodynamic) systems that exhibit transitions from steady to periodic states, and through further periodic and quasi-periodic regimes until the system becomes chaotic (Kimura, Schubert & Straus 1986). The great interest in understanding such behaviour gives additional impetus to finding new and improved methods of analysis that will predict the transition thresholds and that will provide new insight into how they arise.

In this study we employ a modern computational technique for locating the oscillatory instability. The key idea is the recognition that the transition from steady to periodic flow occurs at a Hopf bifurcation in the solution of the steady equations that describe the free convection. This Hopf bifurcation is located by constructing an *extended system* of steady equations whose solution yields the critical parameter values at the bifurcation point; the extra equations added to the original set represent conditions satisfied at the bifurcation. This approach has several advantages over a direct time-dependent simulation. First, the cost of obtaining the critical parameters at the threshold is only of the order of nine times that of solving the steady equations alone. Secondly, the threshold value is predicted exactly, at least to within the limits of truncation error. Thirdly, with standard continuation techniques the variation of the bifurcation point with other parameters can be obtained in a systematic and efficient way. For example, the threshold for oscillations can be determined as a function of aspect ratio. Fourthly, the grid dependence and rate of convergence of the predicted threshold value can be checked readily. Finally, Hopf bifurcations on branches of *unstable* solutions can be located, a capability that is crucial for the interpretation of maps that delineate domains of stability in a two-parameter space.

In a container heated from below, convection begins only when the applied temperature (say) exceeds a critical value defined by linear stability theory. The resulting convection pattern depends both on the magnitude of the temperature difference (or, more precisely, the Rayleigh number Ra) and on the aspect ratio of the cavity. In a study principally concerned with modal exchange mechanisms in the Lapwood problem, Riley & Winters (1989) showed that there is a succession of bifurcations to convective flows, but only the bifurcation with the lowest critical Rayleigh number allows flows that are stable at onset. Their study shows, however, that secondary bifurcations on the other convective branches can stabilize the flows and so lead to multiple stable solutions with differing patterns (which in general comprise differing numbers of horizontal cells, but always with a single vertical cell). The effect of container size was studied by continuation methods in order to determine the variation with aspect ratio of the critical Rayleigh number of the bifurcation points. In this way a stability map was obtained which shows the alternative patterns expected for particular operating conditions. Their stability map, however, is not fully determined, for eventually *each* of the stable modes is destabilized by Hopf bifurcations.

Previous studies of this transition from steady to periodic flow have not brought out this particular feature of multiple destabilization. Caltagirone (1975) identified thermal boundary layers as the source of the destabilizing disturbances. He carried out finite-difference calculations and mapped out a boundary of instability to oscillations as a function of aspect ratio h (width to height). It is unclear from Caltagirone's paper, however, to which mode(s) the boundary corresponds. There is no reason to suppose that, in a cavity of given aspect ratio, each mode undergoes transition at exactly the same Rayleigh number. Aidun & Steen (1987), using an eigenfunction expansion in conjunction with a numerical branch-tracing technique, focused on unicellular flow in a square cavity. They obtained (i) the point of transition, $Ra^{(p)} = 390.7$, (ii) the frequency at transition, $\Omega^{(p)} = 82.8$ cycles per dimensionless time, and (iii) the detailed structure of the destabilizing disturbance. The results (i) and (ii) were also found independently by Kimura *et al.* (1986). In a further study, Steen & Aidun (1988) resolved the form of the destabilizing disturbances for $0.5 \leqslant h \leqslant 1.5$. They carefully constructed one-dimensional fluid-

loop models which clarify the underlying physics of the thermal disturbances. The instability occurs as a travelling wave propagating in a closed loop outside a nearly motionless core; the wave speed is determined by an average base-state velocity, and the spatial structure by a balance between convection and diffusion.

Aidun (1987) considered stability of a unicellular-convection roll in a parallelepiped cavity with a square cross-section. He found that the roll with (dimensionless) axial length $h_1 < 0.115$ destabilizes through the Hopf bifurcation at $Ra^{(p)} = 390.7$. For $h_1 > 0.115$, however, it loses stability to a three-dimensional mode at a lower Rayleigh number.

To summarize this previous work: Caltagirone has mapped out a boundary of instability to oscillations for h lying between 0.1 and 1.5; Steen & Aidun have analysed the thermal-disturbance structure at the onset of oscillatory motion and have calculated transition Rayleigh numbers for h lying between 0.5 and 1.5; Aidun has shown that a roll is first destabilized by a Hopf bifurcation when its non-dimensional axial length is less than 0.115 and the cross-section of the cavity is square. These investigations mainly concern unicellular flow (we believe that Caltagirone's boundary gives the transition point for unicellular flow). There are substantially more studies than the ones cited here, especially notable contributions by Schubert and Straus: Steen & Aidun (1988) make an excellent survey and we refer interested readers to their paper. For brevity, we have concentrated on previous work of immediate relevance to the present study.

Thus we have a good understanding of the steady-to-oscillatory transition for unicellular flow in terms of its location and disturbance structure. There remain, however, open and important questions. What happens to the transition point for unicellular flow when h is greater than 1.5, a regime in which we have already revealed complex exchange mechanisms between stable steady modes? What are the transition points for *multicellular* flows and how do they relate to the multiple steady solutions predicted by Riley & Winters? These are the questions we address in this study.

The plan of the paper is as follows: in §2 the governing equations are formulated, and the underlying symmetries briefly discussed. Then in §3 we describe the numerical techniques used for locating the Hopf bifurcation points. In §4 numerical results are presented, and finally in §5 the findings are summarized.

2. Formulation

2.1. *Problem description*

We consider a two-dimensional rectangular cavity of height H and aspect ratio $h = W/H$, where W is the lateral dimension (width). The cavity comprises a solid matrix of porosity $\tilde{\epsilon}$, permeability K and heat capacity $(\rho c)_s$, saturated by a Darcy fluid with thermal expansion coefficient β, of viscosity ν and heat capacity $(\rho c)_f$. The saturated porous medium is assumed to be in local thermodynamic equilibrium and is taken to have a constant effective thermal conductivity k_* and heat capacity $(\rho c)_*$ where

$$(\rho c)_* = \tilde{\epsilon}(\rho c)_f + (1-\tilde{\epsilon})(\rho c)_s. \tag{2.1}$$

All boundaries are assumed impermeable. The upper and lower boundaries are isothermal at temperatures $T_0 - \frac{1}{2}\Delta T$, $T_0 + \frac{1}{2}\Delta T$, respectively and ΔT is taken to be positive so that the cavity is heated from below; the lateral boundaries of the cavity are adiabatic.

On invoking the Boussinesq approximation, and assuming that the Prandtl–Darcy number is large so that inertia terms may be neglected, convective flows are governed by the dimensionless equations:

$$\nabla^2\psi = -h^{-1}Ra\frac{\partial\theta}{\partial x}, \tag{2.2}$$

$$\nabla^2\theta = \frac{1}{h}\left\{\frac{\partial\psi}{\partial y}\frac{\partial\theta}{\partial x} - \frac{\partial\psi}{\partial x}\frac{\partial\theta}{\partial y}\right\} + \frac{\partial\theta}{\partial t}, \tag{2.3}$$

where (x, y) are the Cartesian coordinates based at the centre of the cavity,

$$\nabla^2 = \frac{1}{h^2}\frac{\partial^2}{\partial x^2} + \frac{\partial^2}{\partial y^2}$$

and ψ, θ are stream and temperature functions, respectively. Here Ra denotes the Darcy–Rayleigh number defined by

$$Ra = \frac{g\beta K\Delta T H(\rho c)_{\mathrm{f}}}{\nu k_*}, \tag{2.4}$$

and quantities have been non-dimensionalized using lengthscales H or W (as appropriate), diffusive velocity scale $k_*/H(\rho c)_{\mathrm{f}}$ and the temperature scale ΔT.

The governing equations (2.2), (2.3) hold in the region

$$\Omega = \{(x, y): -0.5 < x < 0.5, -0.5 < y < 0.5\}, \tag{2.5}$$

while on the boundaries we have

$$\psi = 0, \quad \frac{\partial\theta}{\partial x} = 0 \quad \text{on} \quad x = \pm\tfrac{1}{2}, |y| < \tfrac{1}{2}; \tag{2.6}$$

$$\psi = 0, \quad \theta = \mp\tfrac{1}{2}, \quad \text{on} \quad y = \pm\tfrac{1}{2}, |x| < \tfrac{1}{2}. \tag{2.7}$$

2.2. *Symmetries*

It is straightforward to show that the governing system of steady equations possesses $\boldsymbol{Z}_2 \times \boldsymbol{Z}_2$ symmetry, where the generators of the group are S_x, S_y defined by

$$S_x\begin{pmatrix}\psi\\ \theta\end{pmatrix} = S_x\begin{pmatrix}\psi(x,y)\\ \theta(x,y)\end{pmatrix} = \begin{pmatrix}-\psi(-x,y)\\ +\theta(-x,y)\end{pmatrix}, \tag{2.8}$$

$$S_y\begin{pmatrix}\psi\\ \theta\end{pmatrix} = S_y\begin{pmatrix}\psi(x,y)\\ \theta(x,y)\end{pmatrix} = \begin{pmatrix}-\psi(x,-y)\\ -\theta(x,-y)\end{pmatrix}. \tag{2.9}$$

S_x, S_y and S_xS_y represent left–right, up–down and centro-symmetries, respectively. There exists a pure-conduction solution, viz. $\theta = -y, \psi = 0$, and the bifurcations from this trivial solution have distinct symmetry properties depending on the number of horizontal cells m and vertical cells n. A bifurcation to an odd number of cells in direction j ($j = x$ or y) breaks the symmetry S_j, whilst if $|m-n|$ is odd then the centro-symmetry S_xS_y is broken. In addition to the above symmetries the slip condition in (2.6) implies a translational invariance (Riley & Winters 1989).

A linear stability analysis of the pure-conduction base state, carried out by Sutton (1970) found that eigenmodes exist when the Rayleigh number satisfies

$$Ra_{m,n}(h) = \frac{\pi^2}{(m/h)^2}\{n^2+(m/h)^2\}^2. \tag{2.10}$$

These perturbation eigenmodes represent flows with m horizontal cells and n vertical cells and are given by

$$\Psi_{m,n} = \sin(m\pi\bar{x})\sin(n\pi\bar{y}), \tag{2.11}$$

$$\Theta_{m,n} = -Ra_{m,n}^{-\frac{1}{2}}\cos(m\pi\bar{x})\sin(n\pi\bar{y}), \tag{2.12}$$

where $\bar{x} = x+0.5$ and $\bar{y} = y+0.5$.

From (2.10), we see that the neutral stability curves are geometrically similar in that $Ra_{m,n}(mh) = Ra_{1,n}(h)$. The physical interpretation of this result, which is a consequence of the slip boundary conditions, is simple. The unicellular flow in a cavity of aspect ratio h is identical to one of the cells in the m-cellular flow in a cavity of aspect ratio mh, provided that the Rayleigh numbers are the same.

3. Numerical techniques

3.1. *Extended systems*

We write the time-dependent equations (2.2), (2.3) as

$$\boldsymbol{M}\frac{\partial \boldsymbol{x}}{\partial t}+\boldsymbol{f}(\boldsymbol{x},\lambda,\alpha) = \boldsymbol{0}, \tag{3.1}$$

where $\boldsymbol{f}$ is a smooth nonlinear function, $\boldsymbol{x}$ is the solution vector, λ is the bifurcation parameter Ra, α is the control parameter h, and $\boldsymbol{M}$ is a singular 2×2 diagonal matrix with principal elements $(0, 1)$.

The steady-state form of equation (3.1) is obtained by setting the time derivatives to zero to give

$$\boldsymbol{f}(\boldsymbol{x}_0,\lambda,\alpha) = \boldsymbol{0}, \tag{3.2}$$

where $\boldsymbol{x}_0$ is a steady solution which may be non-unique for certain values of (λ,α). If the solution of the time-dependent equation (3.1) converges to a steady state for large t, then this steady solution is linearly stable and will satisfy the steady equation (3.2). The converse is not true, since steady solutions of (3.2) are not necessarily solutions of (3.1) in the sense that all steady solutions may be unstable to infinitesimally small perturbations. Indeed (3.2) may have solutions at parameter values for which the time-dependent equations possess no realizable steady solution, as in Poiseuille flow in a pipe at large Reynolds number. We shall be concerned in particular with the transition between steady and oscillatory behaviour in the solution of (3.1) as the parameter λ passes through a critical value.

We now describe how the critical value for the oscillatory transition can be found from the steady equation (3.2) alone. Consider the linear stability of the steady solution $\boldsymbol{x}_0$ to a small perturbation $\boldsymbol{x}_1$. By linearizing (3.1) about $\boldsymbol{x}_0$ we find that $\boldsymbol{x}_1$ satisfies

$$\boldsymbol{M}\frac{\partial \boldsymbol{x}_1}{\partial t}+\boldsymbol{f}_x(\boldsymbol{x}_0,\lambda,\alpha)\,\boldsymbol{x}_1 = \boldsymbol{0}, \tag{3.3}$$

and the perturbation behaves as

$$\boldsymbol{x}_1(t) = \epsilon \mathrm{e}^{-\sigma t}\boldsymbol{\xi}, \tag{3.4}$$

where ϵ is the component of $\boldsymbol{x}_1$ along $\boldsymbol{\xi}$ at $t = 0$ and $\boldsymbol{\xi}$ is a generalized eigenvector of the Jacobian matrix $\boldsymbol{f}_x(\boldsymbol{x}_0, \lambda, \alpha)$ with eigenvalue σ given by the generalized eigenvalue problem

$$\boldsymbol{f}_x \boldsymbol{\xi} = \sigma \boldsymbol{M} \boldsymbol{\xi}. \tag{3.5}$$

Thus the steady solution $\boldsymbol{x}_0$ is linearly stable if all the eigenvalues σ have positive real part, but the linear stability changes if one or more eigenvalues crosses the imaginary axis as the parameter λ increases. Since the Jacobian matrix is real it may have both real and complex-conjugate pairs of eigenvalues and there are two different ways in which this loss of stability can occur. First, a real eigenvalue may cross the imaginary axis for increasing λ, so that a value of λ exists at which $\sigma = 0$, the Jacobian matrix is singular, and from the Implicit Function Theorem the uniqueness of $\boldsymbol{x}_0$ is not guaranteed. The critical λ at which this occurs is a singular point of the steady equation (3.2) and bifurcation of the steady solution may occur. Second, a complex-conjugate pair may cross the imaginary axis for increasing λ, so that a value of λ exists at which $\sigma = \pm \mathrm{i}\omega$ and there is an oscillatory solution $\boldsymbol{x}$ of the time-dependent equation (3.1) with angular frequency ω and zero amplitude. The critical value of λ in this case defines a Hopf bifurcation point of the steady equation (3.2), but it should be stressed that the Jacobian matrix is *not* singular and so the solution $\boldsymbol{x}_0$ is unique in the neighbourhood of this point; there is no bifurcation of the *steady* solution $\boldsymbol{x}_0$. Above the threshold for oscillations the steady solution $\boldsymbol{x}_0$ may undergo further Hopf bifurcation as other complex-conjugate pairs of eigenvalues cross into the negative half-plane; although the Hopf points themselves have no physical significance, since $\boldsymbol{x}_0$ is no longer a solution of the time-dependent equation (3.1) at large t, the branches of unstable oscillatory flows to which they give rise may interact with the stable oscillatory mode arising at the lowest bifurcation.

To locate Hopf bifurcations in the steady equations we implement a technique proposed by Jepson (1981) and Griewank & Reddien (1983) in which the following extended set of equations is solved:

$$\begin{pmatrix} \boldsymbol{f}(\boldsymbol{x}_0, \lambda, \alpha) \\ \boldsymbol{f}_x(\boldsymbol{x}_0, \lambda, \alpha)\,\boldsymbol{\xi}_\mathrm{R} + \omega \boldsymbol{M} \boldsymbol{\xi}_\mathrm{I} \\ \boldsymbol{f}_x(\boldsymbol{x}_0, \lambda, \alpha)\,\boldsymbol{\xi}_\mathrm{I} - \omega \boldsymbol{M} \boldsymbol{\xi}_\mathrm{R} \\ \boldsymbol{l}\boldsymbol{\xi}_\mathrm{R} \\ \boldsymbol{l}\boldsymbol{\xi}_\mathrm{I} - 1 \end{pmatrix} = \boldsymbol{0}. \tag{3.6}$$

The functions $\boldsymbol{\xi}_\mathrm{R}$ and $\boldsymbol{\xi}_\mathrm{I}$ are the real and imaginary parts of the right eigenvector of the Jacobian matrix and the last two equations in the set are normalization conditions which use some linear functional $\boldsymbol{l}$ (in our computations we scale the eigenvector so that a fixed component takes the value i). The solution of these nonlinear equations by Newton's method gives successive approximations to $\boldsymbol{x}_0$, $\boldsymbol{\xi}_\mathrm{R}$, $\boldsymbol{\xi}_\mathrm{I}$, λ and ω that converge quadratically to their values at the Hopf bifurcation point $\lambda = \lambda_\mathrm{H}$, for a good-enough initial guess. We compute the variation of the solution with the control parameter α using pseudo-arclength continuation (Keller 1977).

We note from (3.4) that in the neighbourhood of the Hopf point the time-dependent solution behaves as

$$\boldsymbol{x}(t) = \boldsymbol{x}_0 + \epsilon\{\cos(\omega t)\,\boldsymbol{\xi}_\mathrm{R} - \sin(\omega t)\,\boldsymbol{\xi}_\mathrm{I}\}, \tag{3.7}$$

with the amplitude ϵ behaving as $(\lambda - \lambda_H)^{\frac{1}{2}}$ (Joseph & Sattinger 1972). We may use (3.7) with an assumed value of ϵ to visualize the oscillatory flow arising at the Hopf bifurcation.

3.2. *Finite-element approximation*

Following Riley & Winters (1989, 1990), the steady equation (3.2) and the extended system (3.6) were solved in a standard Galerkin form of the finite-element method. The equations were discretized using a grid of nine-node quadrilateral elements with quadratic interpolation for the stream function and the temperature.

The equations were linearized by the Newton–Raphson method, and the algebraic equations for the unknown nodal values were solved directly by a standard frontal method. The cost of solving the extended system (3.6) is of the order of nine times that of solving the steady equations (3.2) alone, with an appropriate two-step Newton–Raphson linearization.

All the computations were carried out on the CRAY-2 at Harwell.

4. Results

Before presenting our new results, it is necessary to set them in the context of our previous work (Riley & Winters 1989, 1990). In figure 1 we reproduce the calculated bifurcation diagram for a square cavity as the Rayleigh number varies. The measure used is the temperature at the mid-point of the left-hand vertical boundary and stable solutions are denoted by solid lines. We see that the unicellular flow is stable from onset at $Ra = 4\pi^2$, the bicellular flow is stabilized by the secondary bifurcation at Ma ($Ra = 81.01$), whilst the tricellular flow is stabilized by the second secondary at UV ($Ra = 160.25$). Along each of the modal branches we expect that there is eventually a Hopf bifurcation which destabilizes these flows. Aidun & Steen (1987), using an eigenfunction expansion and branch-tracing technique (i.e. Doedel's 1981 AUTO package), determined that a Hopf bifurcation occurs at $Ra = 390.7$ along the unicellular branch. They predicted that the angular frequency of oscillations at onset is 520.25 rad per dimensionless time, based on a frequency scale of $k_*/H^2(\rho c)_f$. This is in excellent accord with the independent calculation of Kimura, Schubert & Straus (1987), who used a pseudo-spectral scheme and linear stability analysis. To our knowledge, nobody has calculated corresponding Hopf bifurcation points along the multicellular branches.

In the present study, we first confirmed the location of the Hopf bifurcation along the unicellular branch in a square cavity. The results of our numerical calculations based on five different grids are given in table 1, which also shows the values predicted at zero mesh size through Richardson extrapolation. On the finest grid, both the predicted critical Rayleigh number and angular frequency agree to four significant figures with the results from the computations of Aidun & Steen (1987). In contrast to Aidun & Steen, we found no indication of anything other than a bifurcation of Hopf type at this Rayleigh number, and we found the location of the bifurcation point to be insensitive to the grid resolution in our extended-system approach. Even for the crudest grid we located both the position of the Hopf bifurcation point and the frequency to within 0.5%. Figure 2 shows the streamlines and isotherms of the steady unicellular solution, and the real and imaginary parts of the eigenvector at the bifurcation point, calculated using an 8×8 grid. The steady flow circulates clockwise and accelerates (in a Lagrangian sense) at the upper right and lower left corners under the action of buoyancy forces. The hot upflow (cold downflow) compresses the horizontal thermal boundary layer near the corner. The

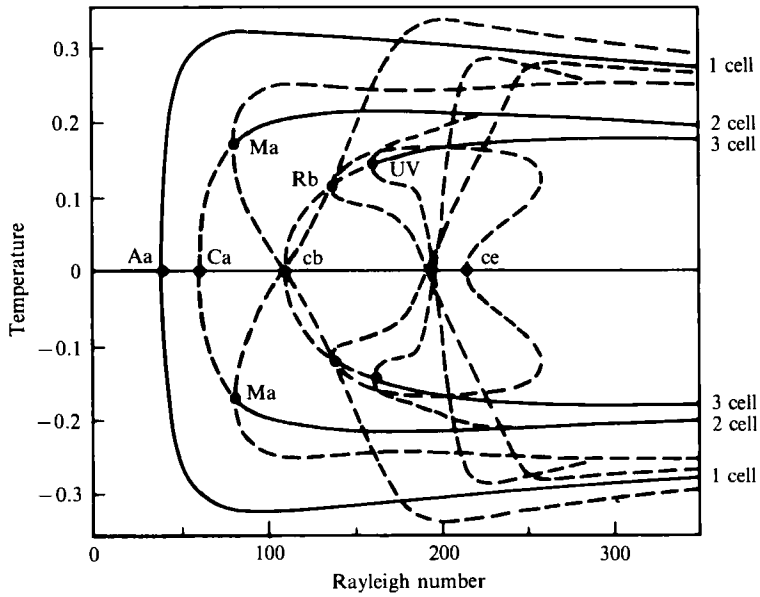

FIGURE 1. Computed bifurcation structure at $h = 1$ showing the three lowest modes. Stable/unstable branches are denoted by full/broken curves. The measure used is the temperature at $(-\frac{1}{2}, 0)$.

Grid	Rayleigh number	Angular frequency
8×8	392.8113	519.371
12×12	391.1723	519.9326
16×16	390.8702	520.1151
24×24	390.7511	520.1709
32×32	390.7309	520.1801
Extrapolated	390.7201	520.1863

TABLE 1. Critical Rayleigh number and frequency at the Hopf bifurcation along the unicellular branch in a square cavity for different grids.

characteristic S-shape in the isotherms shows that they have overturned, leading to a stable stratification in the core which inhibits the flow there. In the eigenvector plots, regions where the disturbances possess positive vorticity (corresponding to clockwise rotation) or positive temperature are delineated by the solid curves. On comparing the real (imaginary) streamline and isotherm plots, we see that the disturbance upflows and downflows generally coincide with positive and negative temperatures, respectively. Given that the directions of the flow and buoyancy forces associated with the disturbances correlate well, one may deduce that the structure of the disturbances is independent of the base flow. This observation by Steen & Aidun (1988) provided the motivation for the fluid-loop modelling that they undertook.

The nature of the oscillatory convection at a Rayleigh number near the critical value may be determined from (3.7). Figure 3 shows the change in the flow and temperature distributions during one oscillation of the periodic 'unicellular' flow in a square cavity. Here the flow is represented by streamlines computed from the

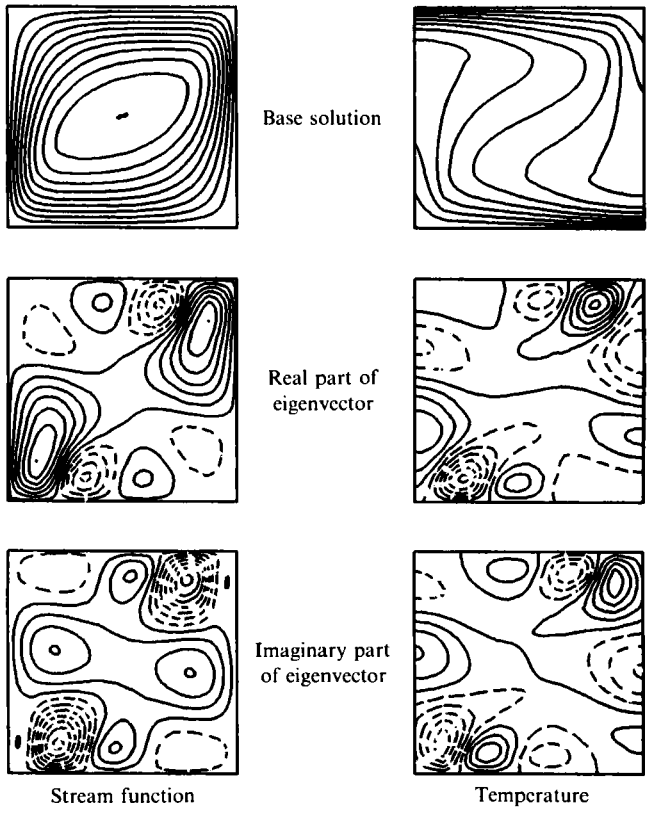

FIGURE 2. Streamlines and isotherms for the steady solution and the real and imaginary parts of the critical eigenvector at the Hopf bifurcation point. Note that the plots are centro-symmetric.

instantaneous velocity field, and ϵ is arbitrarily set equal to 0.11. The visualizations clearly show that, during the cycle, instabilities arise in the thermal boundary layers along the horizontal walls and are advected around the cavity by the base flow. Steen & Aidun showed the evolution of the disturbance structure itself, as defined by $x(t)-x_0$ in (3.7). This evolution (Steen & Aidun 1988, figure 2) is interesting: five thermal disturbances circulate with the base flow outside a nearly motionless core. Moreover, four vorticity disturbances complete a cycle in the same time as the thermals and therefore travel with a 25% greater wave speed; vorticity disturbances pass the thermal disturbances along the adiabatic sidewalls.

In figure 4 we display the predictions, obtained using a 16×16 grid, of the variation with h of the centro-symmetry-preserving Hopf bifurcation point that was located along the unicellular branch at $Ra = 390.7$ when $h = 1$. As we move from $h = 1$ to higher aspect ratio, the locus of the critical Rayleigh number is simple up to $h = 2.4$: the point moves to lower Rayleigh numbers as the aspect ratio increases (figure 4*a*); the associated frequency at onset also decreases, as might be anticipated from energy considerations (figure 4*b*). The computations of Steen & Aidun were carried out for $0.5 \leqslant h \leqslant 1.5$; their results for $h = 1$ and 1.5 agree well with ours and are superposed on figure 4. For $h > 2.4$, however, the structure is more involved and intriguing: a curlicue forms as the path winds back on itself.

To interpret this feature, we first have to review the underlying bifurcation structure of the solution branches. Figure 5 shows schematically the state diagram

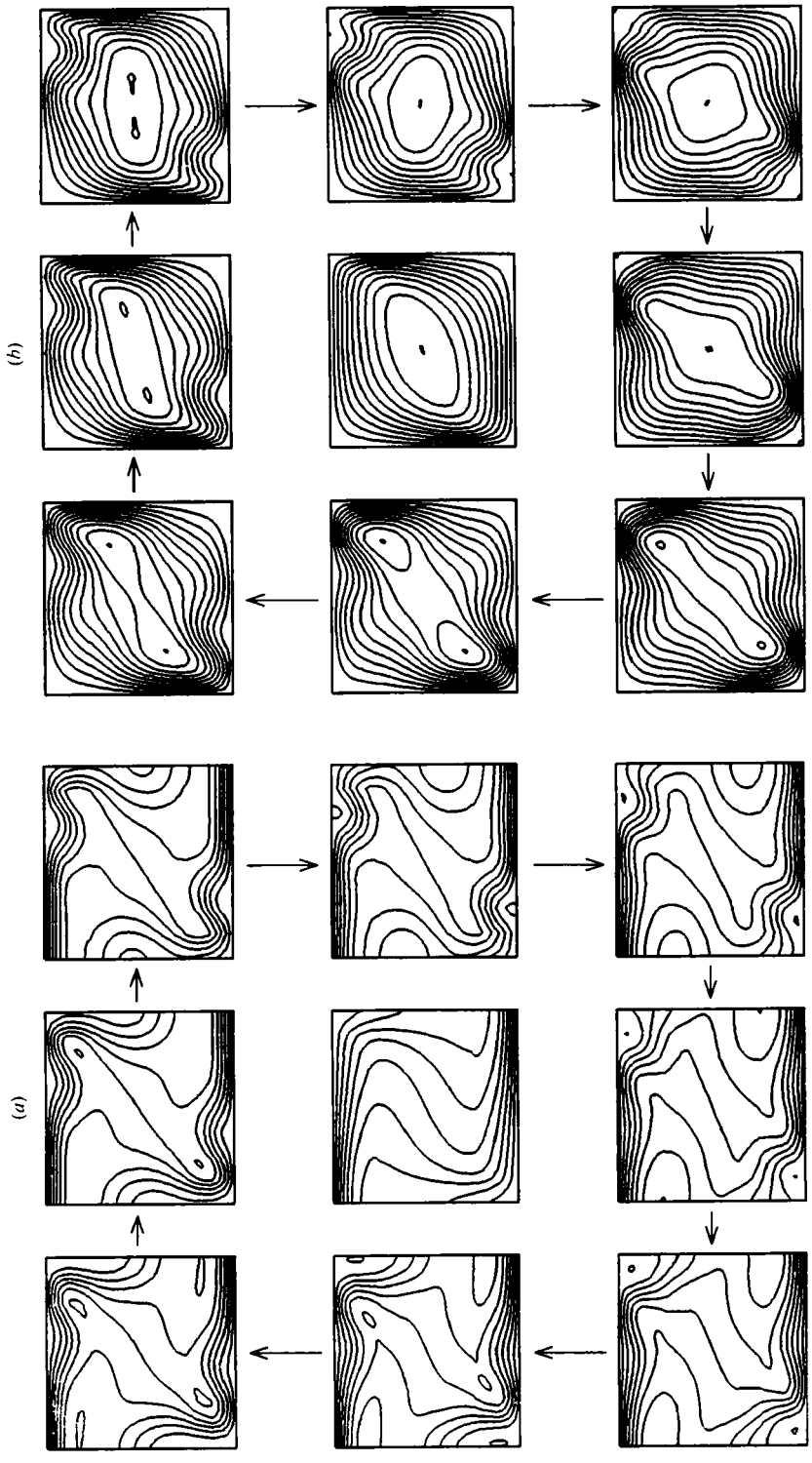

FIGURE 3. Oscillatory disturbances illustrated by instantaneous (*a*) isothermals and (*b*) streamlines at eight equal intervals during one complete cycle, for a value of Rayleigh number near threshold in a square cavity. The visualizations in the centre show the steady-state situation.

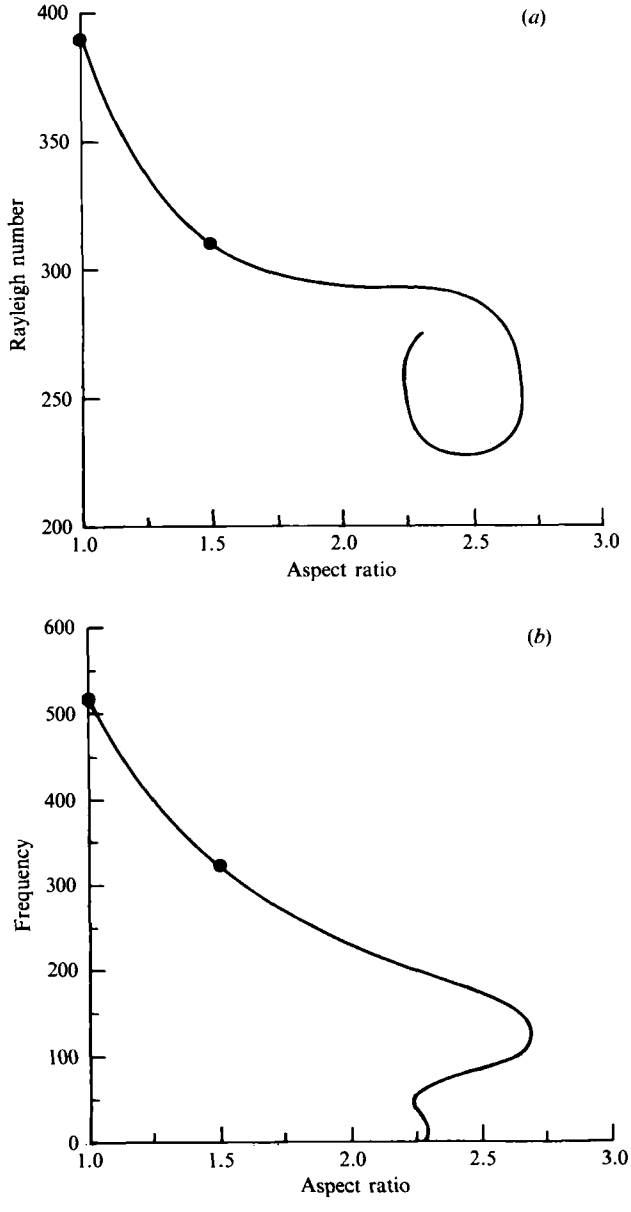

FIGURE 4. (*a*) Computed path of Hopf bifurcation points, (*b*) corresponding variation in angular frequency. The full circles show the calculated results of Steen and Aidun.

that we believe obtains at $h = 2.1$. This particular aspect ratio lies outside the range of our previous investigations, but we have inferred the structure from them and confirmed the most relevant part through new computations. This figure, which displays only those branches connected with the Hopf bifurcation structure, is a composite drawn from the information contained in figures 10, 15(*c*) and 17(*b*) of Riley & Winters (1989) and figure 8 of Riley & Winters (1990). Note that the labelling is the same as in our previous work except for the secondary bifurcations marked s which arise from the exchange between the (1, 1) and (4, 1) modes at $h = 2$. This exchange also accounts for the extra negative eigenvalue on the branches

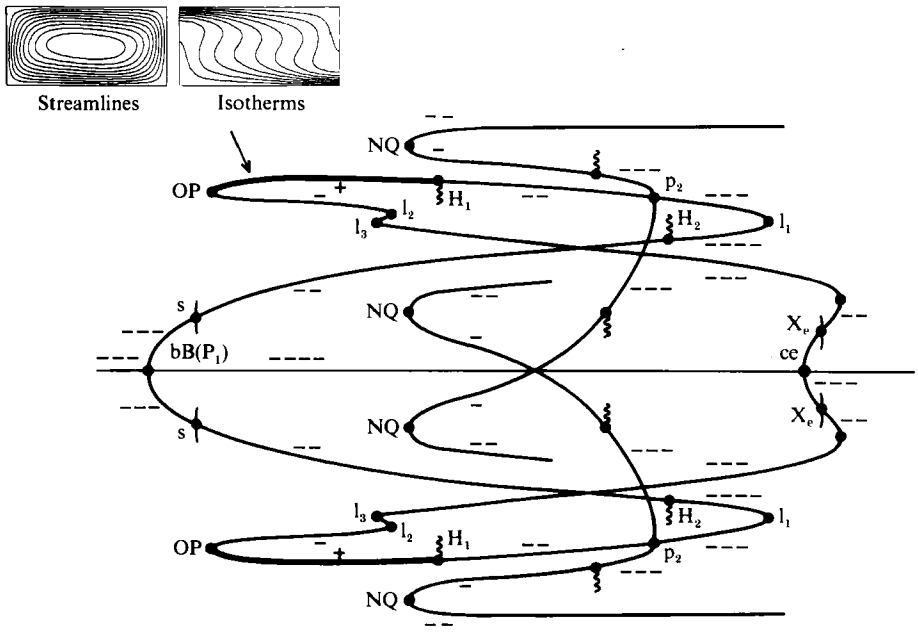

FIGURE 5. Conjectured state diagram when $h = 2.1$. The heavy line between OP and H_1 denotes a stable flow; all other branches correspond to unstable flows.

passing through bB (or P_1) in figure 5 compared with figure 15 of Riley & Winters (1989). Further, the kinks appearing in the branches OPce, together with the associated limit points l_2, l_3, did not feature in this work; we explain their presence below. Stable unicellular flow exists along the branch OPH_1, and the Hopf bifurcation point that we are following is labelled H_1.

To describe how the schema has been determined, we start at $h = 1$ with the computed state diagram, figure 10 in Riley & Winters (1989) (or figure 1 in the present work), together with its conjectured extension to large Rayleigh number, figure 8 in Riley & Winters (1990). Note that this latter figure reflects two assumptions: (i) that the subcritical branches arising at the transcritical secondary bifurcation ($S_{3/1}$) from the three-cell solution merge at the limit point l_1 with the primary one-cell branches, and (ii) that the branches arising at the secondary bifurcation ($S_{2/1}$) from the two-cell solution form a closed loop, and this loop of asymmetric solutions bifurcates from the one-cell branch at the point p_2. Now as h passes through $\sqrt{2}$, the primary one- and two-cell branches swap priority and there is a transfer of the secondaries from the two-cell to the one-cell branches. As h passes through $\sqrt{3}$, the supercritical branches arising at the transcritical secondary bifurcation from the primary three-cell solution and the unicellular branch split and merge, and the resulting mixed branches disconnect, figure 15 in Riley & Winters (1989). The associated subcritical branches form a new primary branch, which we term the one-cell branch since this is the form of the eigenvector of the Jacobian matrix at the bifurcation point. As h increases further, the secondary bifurcation which was on the old one-cell primary branch and is now on the disconnected branch interacts with a tertiary bifurcation which was on the old transcritical secondary branch and the resulting mixed branches disconnect, figure 17 in Riley & Winters (1989). Thus, in figure 5, the limit points OP and NQ arise through the disconnections of the merged primary one-cell and secondary transcritical branches, and the merged

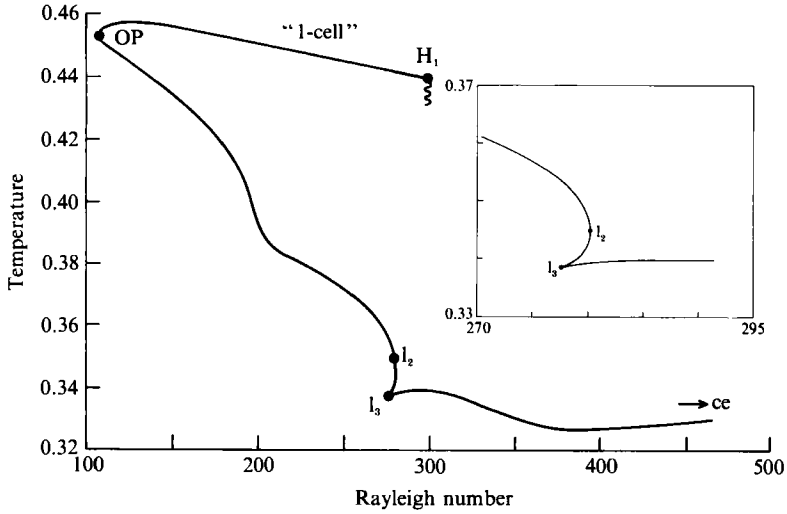

FIGURE 6. Computed state diagram at $h = 2.1$.

secondary and tertiary branches, respectively. The rest of the picture follows from continuity; we have confirmed the new feature in the structure, i.e. the limit points l_2 and l_3, by computing the solution branch $H_1OPl_2l_3$(ce) at $h = 2.1$, as shown in figure 6.

In figure 7(*a*) we have enlarged the view of the curlicue structure shown in figure 4(*a*) and have included paths of singular points necessary for its interpretation, computed on a 16×16 grid. The path OPP′ corresponds to the locus of the limit point OP in figure 5. The paths l_2t and l_3t (see inset) are the loci of the limit points l_2 and l_3 shown in figure 5, which arise when the solution branch buckles at the non-degenerate hysteresis point t, $(h, Ra) = (2.2865, 274.78)$.

We are now in a position to explain the evolution of the state diagram as h increases above 2.1, and the curlicue structure. At the double Hopf point v, $(h, Ra) = (2.236, 258)$, in figure 7(*a*), a pair of Hopf bifurcations H_3, H_4 arises along the solution branch OPl_2 (figure 7*b*). At $(h, Ra) = (2.2848, 274.662)$, the point u in the inset to figure 7(*a*), a further Hopf bifurcation point H_5 is created at the limit point l_2 (figure 7*c*); we find that, as expected, the frequency of oscillation associated with H_5 goes to zero at this Takens–Bogdanov point. We have not indicated the path of homoclinic bifurcations that arises at the Takens–Bogdanov point (Healey *et al.* 1990), but we note that its presence implies complicated dynamical behaviour in the neighbourhood of the point u, with the possibility of chaos being induced through the variation of a second parameter. In this instance, however, such complex effects would appear only in the transient response to a perturbation, if at all, since the Takens–Bogdanov point is located on the unstable part of the solution branch.

Next, as h increases further, the limit points l_2 and l_3 coalesce at the non-degenerate hysteresis point t (figure 7*d*), followed by the coalescence of the Hopf points H_4 and H_5 at the point x (figure 7*e*). Then the Hopf point H_3 tracks towards the limit point OP, and moves around it (figure 7*f*). This features in figure 7(*a*) at P, the osculation point of the limit-point path OPP′ with the path of Hopf bifurcation points $H_3 wH_1$. As h increases further the pair of Hopf points H_1, which has been tracking back towards the limit point OP, and H_3 coincide at the point w, $(h, Ra) = (2.691, 250)$ in figure 7(*a*), as shown in figure 7(*g*). Thus the two Hopf bifurcations interact at w with two possible consequences for the periodic flows

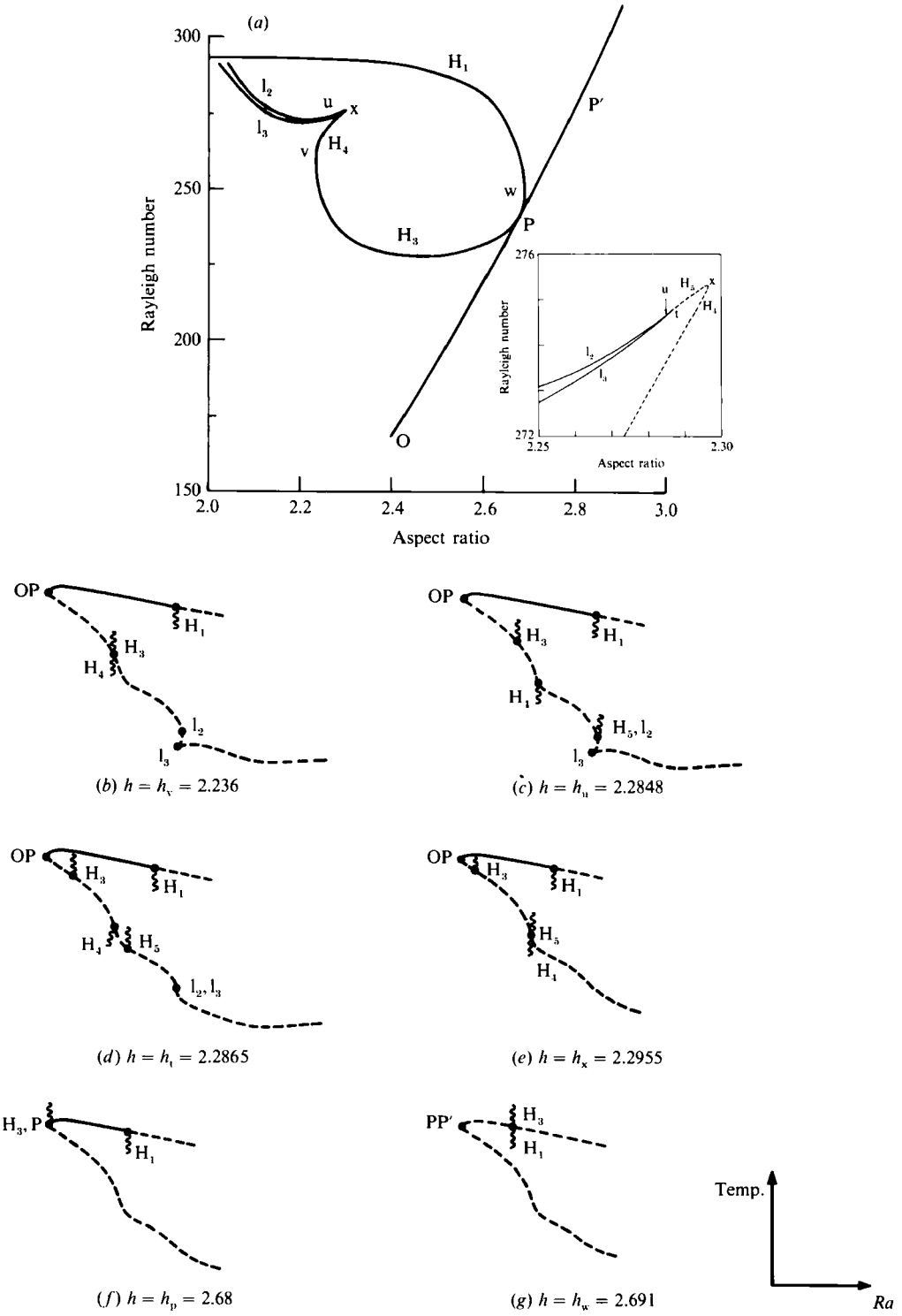

(b) $h = h_v = 2.236$

(c) $h = h_u = 2.2848$

(d) $h = h_t = 2.2865$

(e) $h = h_x = 2.2955$

(f) $h = h_p = 2.68$

(g) $h = h_w = 2.691$

FIGURE 7. (a) Curlicue structure of the Hopf-bifurcation path. For clarity, the paths of Hopf bifurcations are dashed in the insert. (b–g) Schema showing the evolution of the state diagrams as the aspect ratio increases.

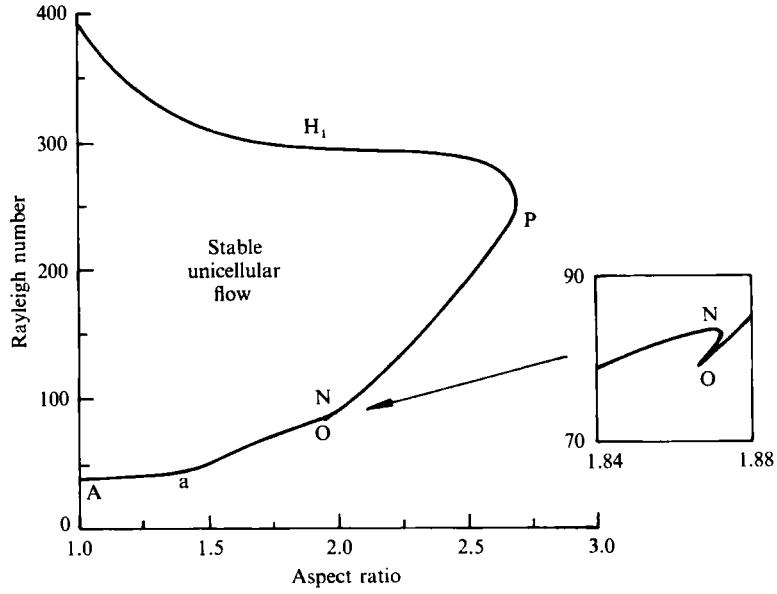

FIGURE 8. Map showing the domain of existence of stable unicellular flow.

Grid	Rayleigh number	Angular frequency
8×8	400.1835	471.039
16×8	392.8113	519.371

TABLE 2. Rayleigh number and frequency at the Hopf bifurcation along the bicellular branch when $h = 2$ for different grids.

arising at these bifurcations: either they are annihilated (at an isola formation point) or disconnected branches of stable periodic flows are formed (at a coalescence point). We do not yet have the computational techniques to resolve these different possibilities. We note that the isola-formation/coalescence points are not double eigenvalues; the time-dependent flow in the neighbourhood of these points is simply periodic.

As regards the steady unicellular flow, it is stable for Rayleigh numbers lying inside the curve $OPwH_1$ in figure 7(*a*). In figure 8 we clarify the domain of existence of stable unicellular flow in (h, Ra)-space. This reveals the unexpectedly complicated shape of the stability boundaries. Clearly, the explanation of such a complex shape can only be found in the analysis of the bifurcation structure of both stable and unstable solutions of the steady-state equations.

We now have a complete description of the stability of unicellular flow to two-dimensional disturbances, but what about multicellular flows? As alluded to in §2, a consequence of the slip-boundary conditions is that the unicellular solution in a square cavity also describes the bicellular flow in a cavity with aspect ratio $h = 2$, the tricellular flow when $h = 3$, and so on. This suggests that, similarly, the symmetry-preserving Hopf bifurcation on the unicellular branch is simply related to those occurring on multicellular branches when h is such that the cells are 'square'.

This indeed turns out to be the case: as we see in table 2, the bicellular branch at $h = 2$ has a (symmetry-preserving) Hopf bifurcation which, if the grids have

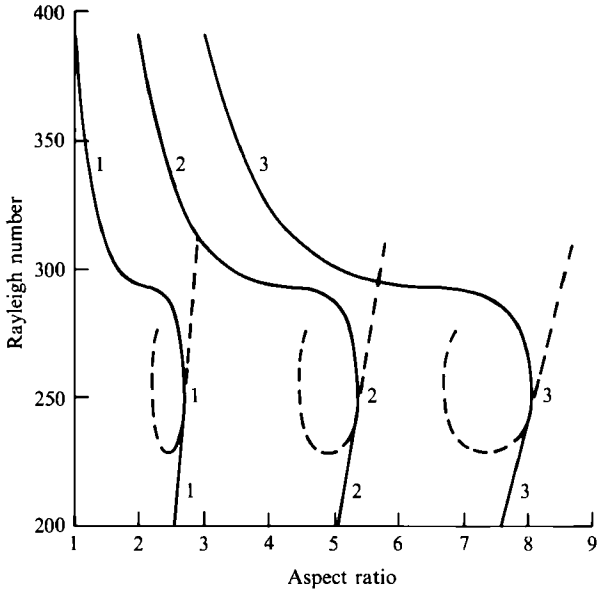

FIGURE 9. Geometrically constructed Hopf-bifurcation paths for the multicellular modes.

equivalent resolution (e.g. 16×8 when $h = 2$ and 8×8 when $h = 1$), is located at exactly the same Rayleigh number as the unicellular Hopf bifurcation at $h = 1$. This geometrical-similarity property generalizes: for a cavity with aspect ratio NH, the N-cellular branch has a symmetry-preserving Hopf bifurcation point at the same Rayleigh number as the symmetry-preserving Hopf bifurcation on the unicellular branch in a cavity with aspect ratio H. Thus we may determine an upper stability limit for the multicellular flows by calculating, as h varies, the locus of the symmetry-preserving Hopf bifurcation point along the unicellular solution branch and then applying the similarity condition; figure 9 shows the result. We should stress, however, that this process only provides *an* upper stability limit. For cavities with $h \sim N$, we believe that, along the N-cellular branch, it is the symmetry-preserving Hopf bifurcation that has the lowest critical Rayleigh number. For other aspect ratios, however, there may be other *symmetry-breaking* Hopf bifurcations with lower critical Rayleigh numbers. Thus we cannot state with certainty that we have calculated *the* upper stability limit for each mode. At the moment, this can only be determined by performing a very expensive full eigenvalue calculation for each solution at each Rayleigh number and aspect ratio.

Aidun (1987) uses a similar geometrical argument in his study of three-dimensional stability of unicellular flow. His results are also subject to the qualification that other instabilities may have onset before the symmetry-preserving ones that he considers.

5. Conclusions

Steady unicellular flow in a square cavity is stable from onset at $Ra = Ra_1^{(s)} \equiv 4\pi^2$ until it is destabilized by a Hopf bifurcation to oscillatory flow at $Ra = Ra_1^{(p)} \equiv 390.7$. As the cavity becomes flatter (larger aspect ratio), the flow becomes less stable: it is realizable (stable) only when $Ra_h^{(s)} < Ra < Ra_h^{(p)}$, where $Ra_1^{(s)} < Ra_h^{(s)}$ and $Ra_h^{(p)} < Ra_1^{(p)}$, that is an increasingly narrow range of Rayleigh number for increasing aspect ratio. Steen & Aidun (1988), in a study mainly concerned with transition mechanisms

per se, followed the position of the Hopf bifurcation until the cavity was 50% longer than it was high, and they confirmed this destabilization. They did not, however, comment on the onset of the unicellular flow after the modal exchange with the bicellular flow at $h = \sqrt{2}$.

In this study, we have followed the paths of the points of onset and destabilization of the steady unicellular flow, and have uncovered a curious structure. On continuing the calculations for values of the aspect ratio greater than 1.5, we discovered that the path of Hopf bifurcations develops a curlicue. After determining the structure of the state diagram we were able to interpret this feature: as the aspect ratio increases, two pairs of Hopf bifurcations arise spontaneously. One of these interacts with a further Hopf bifurcation which arises at a limit point formed by a buckling of the solution branch, whilst the other tracks along the solution branch in the opposite direction. This Hopf bifurcation eventually destabilizes the unicellular flow completely; finally interacting with the original Hopf bifurcation (the one arising at $Ra = 390.7$ in the square cavity), it leaves the unicellular branch. This behaviour determines an upper limit of $h = 2.691$ on the largest aspect ratio for which unicellular flow is stable.

In a cavity of given aspect ratio, stable, steady multicellular flows may exist (Riley & Winters 1989) as alternative states to the unicellular flow usually considered. As far as we are able to ascertain, nobody has addressed the problem of the destabilization of these alternative modes of convection. By employing a simple similarity argument, we generated an upper stability bound for these multicellular flows and we were able to deduce that stable m-cell flows exist only for $h < 2.691m$.

The present technique locates the onset of instability exactly, unlike transient calculations where there may be considerable uncertainty in distinguishing true oscillatory behaviour from transient oscillations which decay to a steady state over a long timescale. A further advantage of the present approach is that, having located a bifurcation point for a particular case (here for unicellular flow in a square cavity), we can obtain by parameter continuation the variation of the critical Rayleigh number and frequency as the aspect ratio varies. The complexity of the stability map for the unicellular flow (figure 8) illustrates that it is only by following unstable, as well as stable, modes that we can obtain the full picture. General time-dependent calculations would not be effective in obtaining this result. A limitation of the present implementation of our numerical techniques is that we are unable to determine whether the Hopf bifurcations are sub- or supercritical. We are currently extending our approach to address this important issue.

The work described here is part of the longer term research carried out within the Underlying Programme of the United Kingdom Atomic Energy Authority.

REFERENCES

AIDUN, C. K. 1987 Stability of convection rolls in porous media. In *Bifurcation Phenomena in Thermal Processes and Convection*. HTD-Vol. 94 and AMD-Vol. 89, p. 31. ASME.

AIDUN, C. K. & STEEN, P. H. 1987 Transition to oscillatory convection in a fluid-saturated porous medium. *J. Thermophys. Heat Transfer* **1**, 268.

BORIES, S. A. 1985 Natural convection in porous media. In *Proc. NATO ASI on Fundamentals of Transport Phenomena in Porous Media*.

CALTAGIRONE, J. P. 1975 Thermoconvective instability in a horizontal porous layer. *J. Fluid Mech.* **72**, 269.

DOEDEL, E. J. 1981 AUTO: a program for the automatic bifurcation analysis of autonomous systems. *Congr. Numer.* **30**, 265–284.

GRIEWANK, A. & REDDIEN, G. 1983 The calculation of Hopf points by a direct method. *IMA J. Numer. Anal.* **3**, 295.

HEALEY, J. J., BROOMHEAD, D. S., CLIFFE, K. A., JONES, R. & MULLIN, T. 1990 The origins of chaos in a modified Van der Pol oscillator. *Physica D* (submitted).

JEPSON, A. D. 1981 Numerical Hopf bifurcation. California Institute of Technology, Pasadena, California, USA.

JOSEPH, D. D. & SATTINGER, D. H. 1972 Bifurcating time-periodic solutions and their stability. *Arch. Rat. Mech. Anal.* **45**, 79.

KELLER, H. B. 1977 Numerical solutions of bifurcation and nonlinear eigenvalue problems. In *Applications of Bifurcation Theory* (ed. P. H. Rabinowitz), p. 359. Academic.

KIMURA, S., SCHUBERT, G. & STRAUS, J. M. 1986 Route to chaos in porous medium thermal convection. *J. Fluid Mech.* **166**, 305.

KIMURA, S., SCHUBERT, G. & STRAUS, J. M. 1987 Instabilities of steady, periodic and quasi-periodic modes of convection in porous media. *Trans. ASME* C: *J. Heat Transfer* **109**, 350.

RILEY, D. S. & WINTERS, K. H. 1989 Modal exchange mechanisms in Lapwood convection. *J. Fluid Mech.* **204**, 325.

RILEY, D. S. & WINTERS, K. H. 1990 A numerical bifurcation study of natural convection in a tilted two-dimensional porous cavity. *J. Fluid Mech.* **215**, 309.

STEEN, P. H. & AIDUN, C. K. 1988 Time-periodic convection in porous media: transition mechanism. *J. Fluid Mech.* **196**, 263.

SUTTON, F. 1970 Onset of convection in a porous channel with net through flow. *Phys. Fluids* **13**, 1931.